Available online at www.sciencedirect.com

ScienceDirect

www.elsevier.com/locate/matchar

Characterization of a Messer – The late-Medieval single-edged sword of Central Europe

Peter Fajfar[a], Jožef Medved[a], Grega Klančnik[a], Tomaž Lazar[b], Marijan Nečemer[c], Primož Mrvar[a,*]

[a]Department of Materials and Metallurgy, Faculty of Natural Sciences and Engineering, University of Ljubljana, Aškerčeva cesta 12, SI-1000 Ljubljana, Slovenia
[b]National Museum of Slovenia, Prešernova cesta 20, SI-1000 Ljubljana, Slovenia
[c]Jožef Stefan Institut, Jamova cesta 39, SI-1000 Ljubljana, Slovenia

ARTICLE DATA

Article history:
Received 29 April 2013
Received in revised form
3 October 2013
Accepted 6 October 2013

Keywords:
Iron
Steel
Blacksmith
Archaeometallurgy
Medieval sword
Microstructural characterization

ABSTRACT

Metallurgical characterization of a sword blade fragments dating from the second half of the 15th century found in central Slovenia was performed in order to determine its chemical composition, microstructure, microhardness, and to obtain insight into the methods of manufacture of a late-medieval Messer sword. As the artefact was broken, examinations were limited to six very small fragments that were allowed to be removed from the cutting edge, core and the back of the blade. Light optical microscopy, scanning electron microscopy, energy dispersive X-ray spectroscopy, energy dispersive X-ray fluorescence spectrometry, differential scanning calorimetry, thermodynamics approach and Vickers micro-hardness tests were employed to analyze the microstructure and mechanical properties. The results show that the sword was manufactured from a single wrought iron billet. The surface of the sword was carburized. No evidence of quenching was found. The ferritic microstructure is concentrated in the core, and the pearlitic in the outer layer of the blade. All metal fragments contained non-metallic inclusions that were derived mostly from slag and some from hammer scale.

1. Introduction

The so-called Messer was a distinct Central European weapon that enjoyed great popularity in the 15th and 16th centuries. Its nondescript name, meaning simply 'knife' in German, applied to a wide family of one- or two-handed swords. Generally, the 'Messer' can be defined as a cutting sword with a straight or slightly curved single-edged blade. It was usually fitted with a cruciform hilt provided with a small lug on the right side to protect the user's hand. But it was the construction of the grip that separated it from most contemporary 'knightly' swords. The 'Messer' had no massive pommel to counterbalance the weight of the blade. Instead, its grip was designed much like that of an ordinary knife, with a full tang and grip scales made of wood or horn [1–5].

These long fighting 'knives' were once common throughout central Europe and beyond, from the Low Countries to Eastern Europe and the Balkans. Their use was taught by famous fencing masters [6,7] (Fig. 1). They were even depicted regularly by such famous artists as Albrecht Dürer and Pieter Bruegel the Elder [8]. Yet for all its historical importance, the Messer remains relatively unknown and poorly understood. Whereas the medieval double-edged sword has been the subject of numerous studies, very little solid research has been published on the Messer [9]. Without doubt, this can be largely attributed to the Messer's modest origins. It was a weapon of the masses,

* *Corresponding author*. Tel.: +386 41 835530; fax: +386 1 4704560.
E-mail address: primoz.mrvar@omm.ntf.uni-lj.si (P. Mrvar).

1044-5803/$ – see front matter © 2013 Elsevier Inc. All rights reserved.
http://dx.doi.org/10.1016/j.matchar.2013.10.005

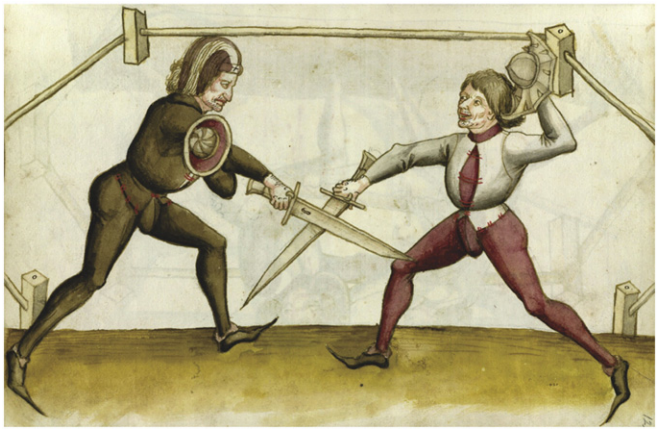

Fig. 1 – Fencing with the Messer as depicted in Hans Talhoffer's fighting manual from 1459 (Det Kongelike Bibliotek København, Thott 290 2°, fol. 122r).

not the aristocratic elite, and would not have appealed to later generations nearly as much as the iconic knightly sword.

Clearly, the Messer had always been a plain sidearm of little symbolic value. This explains why few reasonably intact originals survive to this day — they were simply not considered valuable enough to be treasured for later generations. However, many more examples have been uncovered archaeologically, attesting to its widespread use. In the collection of the National Museum of Slovenia (Narodni muzej Slovenije) alone, there are several dozen long 'fighting knives' from the 15th and early 16th century. However, for the most part, the results of the research of the collection have not been systematically published to this date [10]. One of these swords, hitherto unpublished, is catalogued under inventory number N 32526 and is quite typical of its kind. It entered the museum's collection around 1908, apparently as a chance find from the village of Spodnje Bitnje near Kranj. The site lies in the North West part of central Slovenia (Fig. 2). The sword cannot be dated with absolute precision, but seems relatively consistent with a Messer from the second half of the 15th century, based on a typological analysis and comparison with similar archaeological finds from a dated context. A similar sword with a broken blade of nearly identical length has also been found in Celje, dating from the same period [11] as the sword investigated.

It is often assumed that the Messer was a cheap weapon made by unskilled local labour using inferior materials. However, a closer look at the originals often reveals surprisingly good workmanship — evenly forged, straight, beautifully tapering blades that could only have been produced by experienced craftsmen.

The primary aim of the research was to establish whether the Messer was made from quality steel or merely inexpensive wrought iron, how it was forged – from a single billet or multiple metal bars of varying content – and whether it was subjected to an effective heat treatment. Answers to the above questions may seem quite technical in nature but their implications are wide-ranging, for they may well help to explain the Messer's actual role in the social and cultural context of late-Medieval central Europe [12–14].

Fig. 2 – The location of Spodnje Bitnje.

2. Experimental

The overall length of the weapon is now 493 mm, of which the surviving portion of the blade measures 372 mm (Fig. 3). It weighs 748 g. The single-edged blade is straight and quite wide, 52 to 44 mm, with a flat V-shaped cross-section. The back of the blade is 7.5 mm thick at the hilt but tapers quickly to just 2.4 mm at the fracture point. There is a small maker's mark stamped on the left side of the blade in the shape of a Latin cross, although at this stage it is impossible to safely attribute it to any documented workshop (Fig. 3). The tang is stout and relatively short, with three round holes for securing the now missing grip scales. The hilt consists of a massive crossguard 145 mm in length decorated with a pair of incised rings on each arm. Typically for the central European Messer,

Fig. 3 – Broken Messer from the National Museum of Slovenia showing the location of samples (Photo: Tomaž Lauko, Tomaž Lazar, National Museum of Slovenia, inv. no. N 35256).

the crossguard is fixed to the tang with a round rivet that extends into a curved parrying lug on the right side of the hilt.

The blade is broken. It can be estimated that about half of its original length is missing. Nonetheless, the rest of the weapon is reasonably well preserved.

2.1. Non-destructive methods

For chemical analysis of the sword, energy dispersive X-ray fluorescence spectrometry (EDXRF) was used. The locations of the EDXRF measuring are given in Fig. 4. The Cd-109 radioisotopic disc source was mounted in a holder which was placed on a vertical Si(Li) detector. The artefact was placed on the holder and the area of the sample analysed was 0.6 cm^2. Fluorescent radiation was excited in the samples by the 10 mCi excitation source of Cd-109 from Isotope Products Laboratories, U.S.A. The fluorescence radiation emitted was measured by an energy dispersive X-ray spectrometer composed of a Si(Li) detector (Ortec EG&G), a spectroscopy amplifier (Canberra M2025), an ADC (Canberra M8075) and a PC-based MCA (S-100, Canberra). The energy resolution of the spectrometer was 175 eV at 5.9 keV. Analysis of the complex X-ray spectra was performed by the AXIL spectral analysis program [15]. The program yields the intensities of fluorescent as well as of scattered lines. Quantification of the content of metals after the necessary calibration of the EDXRF system was then performed by the quantitative analysis of environmental samples (QAES) software developed in our laboratory [16].

Thermo-Calc software was used to predict the possible existence of fayalite in the non-metallic inclusions and for calculation of the Fe–Fe_3C phase diagram.

2.2. Destructive methods

Small samples (approximately 2 mm × 2 mm) (Fig. 5) were removed from the core (1), cutting edge (2) and back (3) of the blade (Fig. 3). The samples marked 'a' in Fig. 3 were used for thermal analysis, using differential scanning calorimetry (DSC) and those marked 'b' in Fig. 3 for metallurgical analysis. The samples 1a and 1b were cut in the transverse direction, the samples 2a and 2b were cut in the longitudinal direction and the samples 3a and 3b at a 45 degree angle perpendicular to planar section according to the ASTM-E3 Standard (Fig. 6). They were mounted using VAriDur 200 Buehler cold mounting compound, and then grinded on paper of decreasing grain size of 400, 600, 800, 1200 to 2400. Further preparation of the metallographic specimen included polishing with 3-micron diamond abrasive, followed with 1-micron suspended aluminium oxide and the final polishing with 0.15 micron diamond abrasive, and etched with Nital (a solution of 2 vol.% HNO_3 in ethanol).

Fig. 4 – Locations of EDXRF measuring.

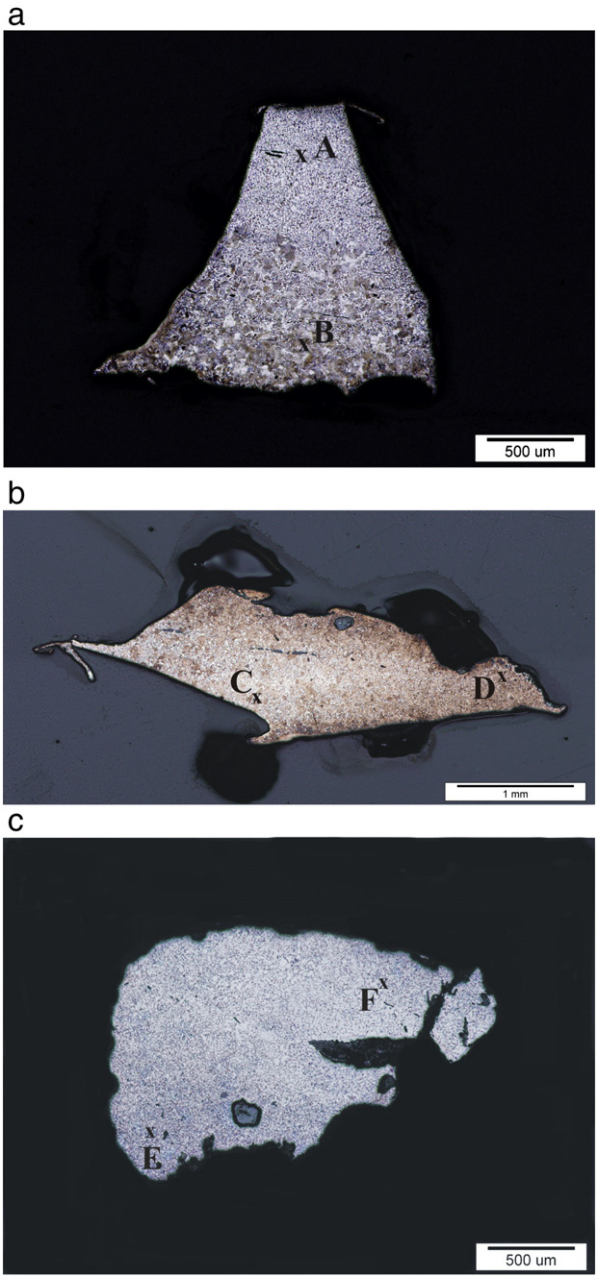

Fig. 5 – Location and orientation of removed samples.

The microstructure was investigated using light optical microscopy (Olympus Microscope BX61) and a Jeol-JSM6500F scanning electron microscope (SEM).

The size, shape and chemical composition of the non-metallic inclusions were defined using the SEM equipped with an energy-dispersive X-ray spectroscope (EDS).

Thermal analysis is a widely used experimental method intended mainly for microstructure and sample history study [17]. Microstructural changes, as well as sample history, have an influence on the measured DSC response. DSC was performed using an STA 449c Jupiter, Netzsch apparatus in a corundum crucible. Measurements were performed in a protective atmosphere of argon 5.0. Samples were heated and cooled at a

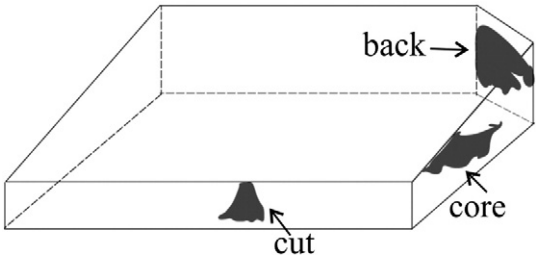

Fig. 6 – Schematic showing locations of examination: (a) cutting edge; (b) core; (c) back.

rate of 10 K min^{-1} since lower heating/cooling rates could lead to decarburization of the samples.

A Vickers micro-hardness instrument Instron Wilson-Wolpert Tukon 2100B was used to indicate differences in micro-hardness values of the samples. The load used was set to 300 g.

3. Results

3.1. *Energy dispersive X-ray fluorescence spectrometry (EDXRF)*

In order to obtain the general chemical composition of the sword, the EDXRF measurements were carried out at different parts of the sword (Fig. 4). Four measurements were carried out on the blade in the middle (points 1 and 2), the edge (point 5) and the back (point 6), two on the tang (points 7 and 8), and a single measurement on the crossguard and on the rivet. The chemical composition of the blade measured by EDXRF is given in Table 1. The results confirmed that the dominant element in the sword was iron (94.4–99.9 wt.%). Other elements found in the sword were zinc (0.6–2.6 wt.%), copper (0.2–0.6 wt.%), lead (up to 1.0 wt.%) and calcium (0.1–0.2 wt.%).

The evaluated uncertainty of this procedure included the statistical uncertainty of the measured intensities and the uncertainty of the mathematical fitting procedure. The overall uncertainty of spectral measurement and analysis was in most cases between 5 and 10%.

Table 1 – Chemical composition of investigated blade by EDXRF (wt.%).

	Composition weight percentage (wt.%)				
Point	Fe	Cu	Zn	Ca	Pb
1	99.9	0.3	0.7	0.1	0.1
2	96.8	0. 6	1.2	0.1	0.1
3	97.4	0.4	0.6	0.1	0.1
4	97.1	0.2	0.6	0.2	0.1
5	96.7	0.2	1.6	0.1	1.0
6	96.8	0.3	1.0	0.2	0.2
7	97.5	0.3	0.7	0.1	0.1
8	94.4	0.4	2.6	0.2	0.9

3.2. *Light optical microscopy (LOM)*

Each of three samples was investigated at two sites (A–F). Marks A, C, D and E are located at the surface layers, while marks B and F are located towards the inside of the blade (Fig. 5).

Fig. 7 shows the microstructures of samples of the investigated artefact. The fractions of total ferrite and pearlite phases are listed in Table 2. In the outer layers of the blade pearlite is the dominant microstructure constituent (Fig. 7b–d), while in the core of the blade mainly ferrite was found (Fig. 7a, e). In the microstructure of the back, close to the core of the blade (Fig. 7f) 47% ferrite and 53% pearlite were found. It was observed that the ferritic structure is gradually converted into the pearlitic structure (Fig. 8).

3.3. *Scanning electron microscopy with energy dispersive X-ray spectroscopy (SEM-EDS)*

The chemical composition of the blade at two characteristic locations (cutting edge and core) of the blade was obtained by SEM-EDS analysis (Fig. 9). Traces of aluminium were found. The quantitative phase analyses performed on backscattered micrographs revealed that the cutting edge of the blade contains a higher amount of carbon than the core.

The non-metallic inclusions found in this study were of two shapes, namely as lumpy ones (Fig. 10a) or as elongated strings (Fig. 10b). The chemical composition of the non-metallic inclusions is given in Table 3. Samples 1–3 correspond to the lumpy inclusions, while the samples 4–7 correspond to the elongated inclusions. The lumpy inclusions are enriched mainly on FeO. Such inclusions are hard and susceptible to cracking during hammering. This implies that the (pressure) ratio of CO_2(g)/CO(g) by reduction was such that equilibrium between FeO/Fe was reached before complete ore reduction and that the inclusions were already present in the wrought iron. Reactions involved in the reduction of iron ore are as follows: $Fe_2O_3 \rightarrow Fe_3O_4 \rightarrow FeO \rightarrow Fe$. The correlation of $p_{CO2}(g)/p_{CO}(g)$ will be given further in this paper. Some of inclusions, enriched in SiO_2, were plasticized and elongated in the direction perpendicular to the direction of hammering (Fig. 10b).

3.4. *Differential scanning calorimetry (DSC)*

DSC was used for investigation of the phase transitions occurring as a consequence of heating small samples taken from the investigated artefact. A series of endothermic peaks was found on heating the samples to 1550 °C. The DSC curves are represented in Fig. 11. The DSC heating curves obtained reveal the complexity of the investigated sample which was already evident from the microstructural observations. First the endothermic peak at approximately 727 °C, found in all three samples, matches the calculated Fe–Fe_3C phase diagram and is related to the eutectoid phase transformation, denoted as temperature A_1. The second, less intense, peak is in agreement with the temperature A_3 confirming the presence of pro-eutectoid ferrite in the lower carbon region. Some of the absorbed heat can be attributed to the magnetic transition of ferrite. At approximately 1000 °C, energy is absorbed for dissolution of secondary cementite present on grain boundaries in the carbon enriched regions. From 1000 °C there is also

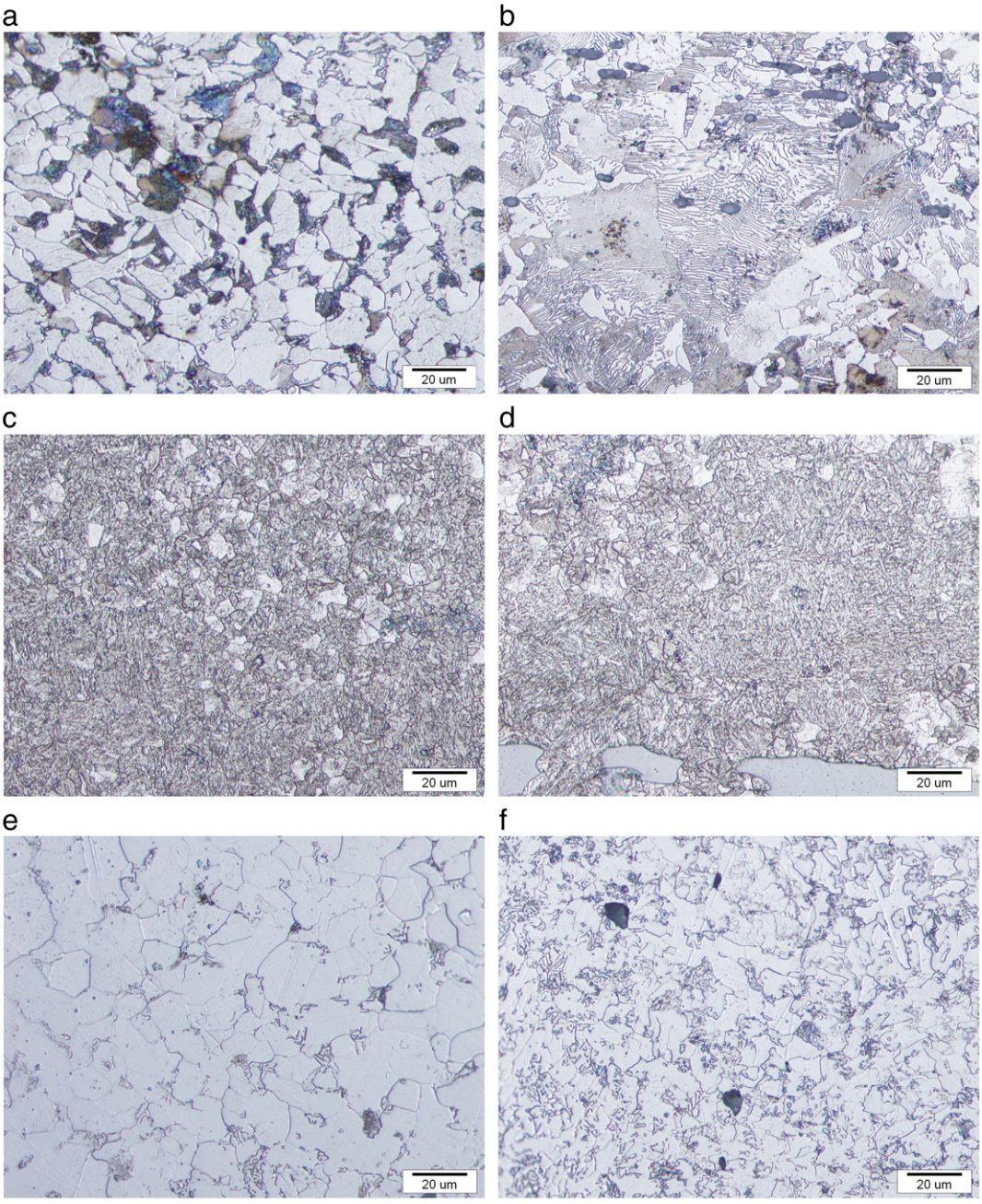

Fig. 7 – Optical micrographs of the investigated blade: (a) cutting edge, point A; (b) cutting edge, point B; (c) core, point C, (d) core, point D; (e) back, point E; (f) back, point F.

exothermic release of stored energy (from hot-cold hammering) for the recovery and recrystallization of austenite grains. The very intense main peaks, at approximately 1360 °C and 1530 °C, represent the melting of the primary austenitic and delta ferritic phases, respectively. The temperature at approximately 1400 °C could be related somehow to the reaction γ-iron → δ-iron allotropic point (A_4) at 1394 which is typical for relatively pure iron, denoted as A_4.

Table 2 – The fractions of total ferrite and pearlite phases (Fig. 4).

Mark	Ferrite	Pearlite
A	0.81	0.19
B	0.22	0.78
C	0.10	0.90
D	0.06	0.94
E	0.68	0.32
F	0.47	0.53

3.5. *Microhardness measurements*

Vickers microhardness tests were performed on samples removed from the artefact (Fig. 5a–c). For each location five measurements were carried out and the average values were calculated, as shown in Table 4. The microhardness of the samples varied between 151 HV and 377 HV. The average

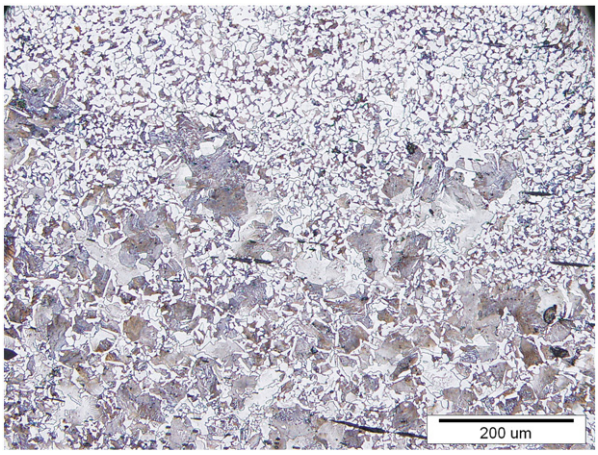

Fig. 8 – Optical micrograph of the region where a mainly ferritic microstructure is converted to a mainly pearlitic one (at the cutting edge).

microhardness of the sample 1 (the edge) was 220 HV, of the sample 2 (the core) 353.8 HV, and of the sample 3 (the back) 190 HV.

4. Discussion

In the present work, non-destructive and destructive testing was used to characterize the chemical composition, the structure, the non-metallic inclusions and the microhardness of the medieval sword.

Since the artefact belonged to the national heritage, the metallurgical investigations allowed were of limited scope. To define the overall chemical compositions of the sword, the EDXRF method was used, which is the most widely used non-destructive method in archaeology [18–21]. The presence of copper and zinc seemed somewhat surprising at first. However, it might be explained as a later contamination. In the past, brass brushes were commonly used at the National Museum of Slovenia for cleaning metal, particularly iron objects. This process could leave a small residue on the surface of the object. To confirm the theory, several test plates of homogeneous low-carbon steel (St 37) were exposed to manual and machine cleaning with brass brushes. XRF measurements indeed detected similar quantities of copper and zinc. Clearly, the presence of copper and zinc on the knife blades must be attributed primarily to recent conservation procedures.

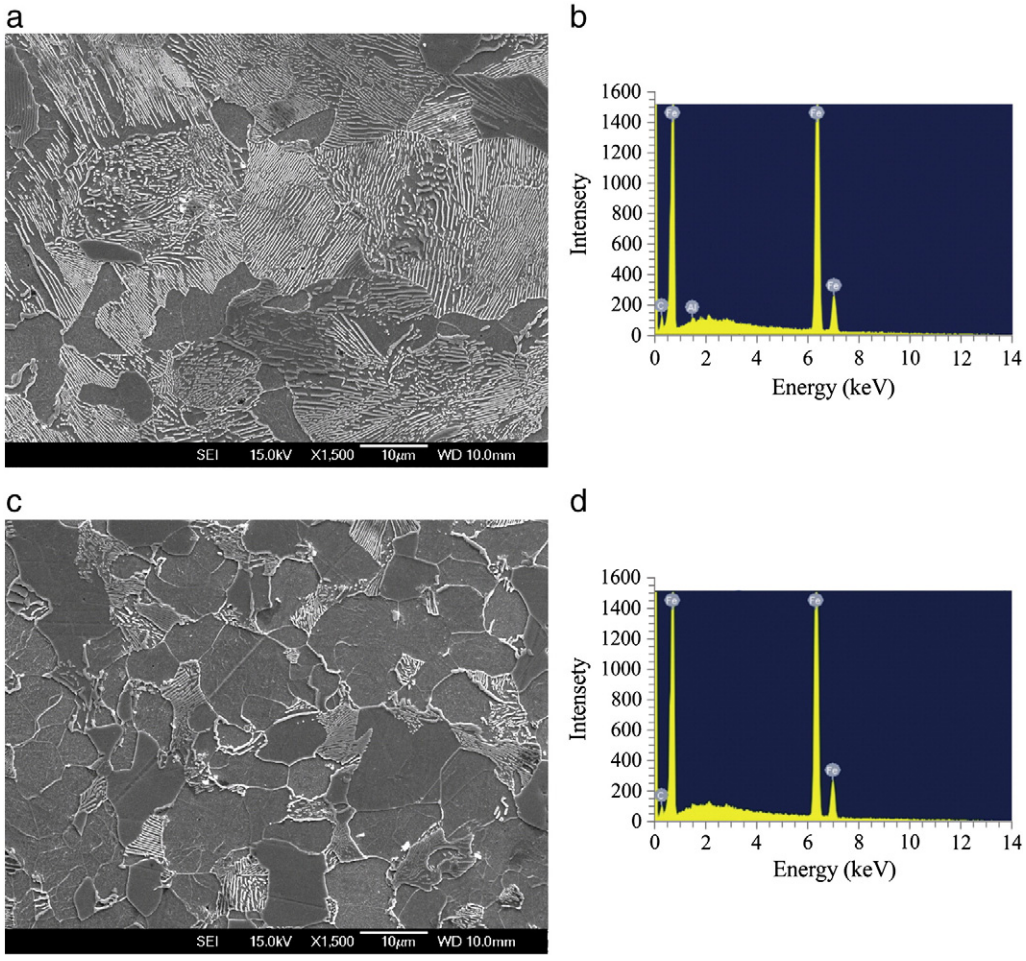

Fig. 9 – SEM micrographs of investigated blade and related EDS spectra. (a) Microstructure of the cutting edge of the blade is mainly pearlitic. (b) Corresponding EDS spectra of the mainly pearlitic microstructure. (c) Microstructure of the blade core is mainly ferritic. (d) Corresponding EDS spectra of the mainly ferritic microstructure.

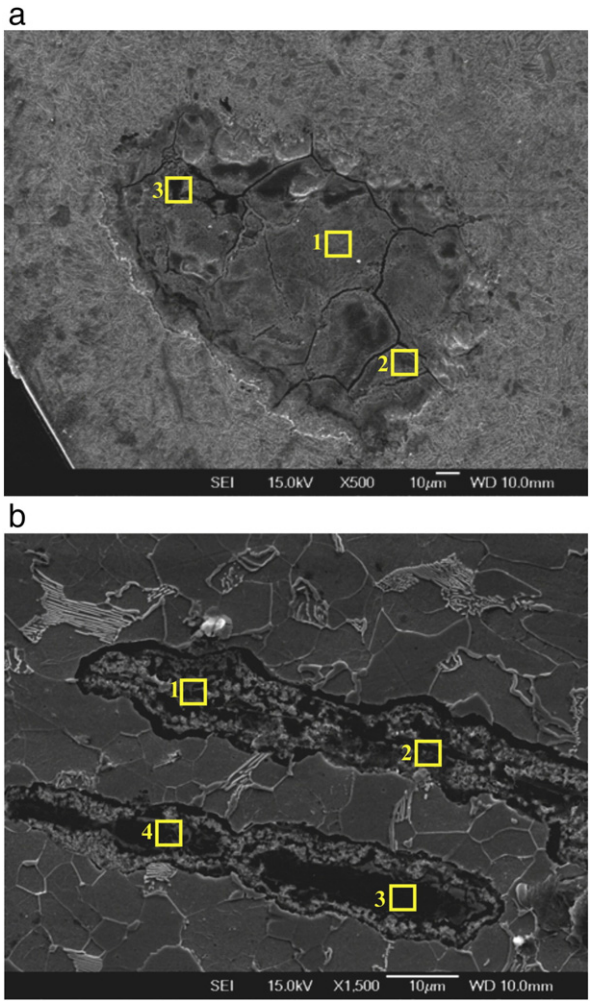

Fig. 10 – SEM micrographs of non-metallic inclusions. (a) Lump shaped non-metallic inclusion; (b) Deformed elongated non-metallic inclusions.

In addition to non-destructive analyses, the destructive ones enabled a deeper insight into the technology of the late-Medieval Messer production [22]. In general, destructive analyses such as metallography are undesirable for museum objects, which must be carefully preserved for posterity. However, in this particular case the structure of the blade had already been exposed along the fracture line. This allowed us to carefully remove nearly microscopic fragments from the cutting edge (Fig. 5a), core (Fig. 5b) and the back (Fig. 5c) of the blade for further study without causing undue damage.

Table 3 – Chemical composition of non-metallic inclusions (wt.%).

Sample	Composition weight percentage (wt.%)						
	SiO_2	CaO	FeO	Al_2O_3	MgO	MnO	ZnO
1	1.4	0.5	93.8	0.0	0.0	0.0	4.3
2	3.3	0.6	93.6	0.0	0.0	0.0	2.5
3	52.6	14.9	10.5	12. 5	4.1	5.4	0.0
4	2.1	0.6	90.9	6.4	0.0	0	0.0
5	6.0	1.2	80.6	9.8	0.0	2.4	0.0
6	13.8	43.0	26.0	6.5	0.0	10.8	0.0
7	48.8	9.3	9.9	8.2	3.6	21.2	0.0

The sword is heavily and unevenly corroded. Therefore, the investigated surface actually represents the microstructures in different layers of the original blade geometry. This is why the results must be carefully interpreted.

In the current investigation no distinct multilayer structures were observed. These facts indicate that the blade was probably made from a single wrought iron billet. To achieve the required mechanical properties of the blade – a hard outer layer and a tough core – the billet was placed into carbonaceous material after forging. At a sufficiently high temperature the austenite phase was enriched with carbon which diffused from the outer layers. Afterwards the blade was air cooled, resulting in equi-axial grains. If the sword had been fabricated below the critical temperature (A_1), elongated grains would have been expected.

The presence of non-metallic inclusions in the medieval bloom of iron was a normal phenomenon [23,24]. The relation between slag, ore and inclusions in bloom is a very complex one. Three main inclusions are possible. The so-called smelting inclusions are produced by direct ore reduction (enriched on FeO). The modified smelting inclusions could be formed due to interactions with the hammer scale, and/or due to preparation of the surface before welding using siliceous sand (formation of fayalite $2FeO.SiO_2$). If the workpiece was folded and then forge-welded during hammering, then bi-phase structures of inclusions with FeO in the centre and layered by $2FeO.SiO_2$ would be found [25].

In the manufacture of wrought iron, Fe(s), iron ore is reduced by CO(g) where CO(g) can also be oxidized to CO_2(g). From the thermodynamic point of view, the pressure ratio between CO_2(g)/CO(g) has an important role in the efficiency of manufacturing relatively pure Fe(s), regardless of the type of furnace. To achieve equilibrium between FeO(s), Fe(s), CO(g) and CO_2(g), the total Gibbs energy (G_{Total}) of the smelting system is the sum of all the partial Gibbs energies ($\bar{G}$):

$$G_{Total} = n_{Fe}\bar{G}_{Fe} + n_{FeO}\bar{G}_{FeO} + n_{CO}\bar{G}_{CO} + n_{CO2}\bar{G}_{CO2} \quad (1)$$

After differentiation and taking the Gibbs–Duhem equation into account:

$$dG_{Total} = \bar{G}_{Fe}dn_{Fe} + \bar{G}_{FeO}dn_{FeO} + \bar{G}_{CO}dn_{CO} + \bar{G}_{CO2}dn_{CO2} = 0 \quad (2)$$

where the partial Gibbs energy is:

$$\bar{G}_i = G_i^0 + RT\ln a_i \quad (3)$$

and i = FeO, Fe, CO and CO_2. R is the molar gas constant and T temperature. The activity of a species is described by $a_i.G_i^0$ represents the standard Gibbs free energy (pure state).

Considering the mass balance:

$$dm_{Fe} = 0 = dn_{Fe} + dn_{FeO} \quad (4a)$$

$$dm_C = 0 = dn_{CO} + dn_{CO_2} \quad (4b)$$

$$dm_O = 0 = dn_{CO} + 2dn_{CO2} + dn_{FeO} \quad (4c)$$

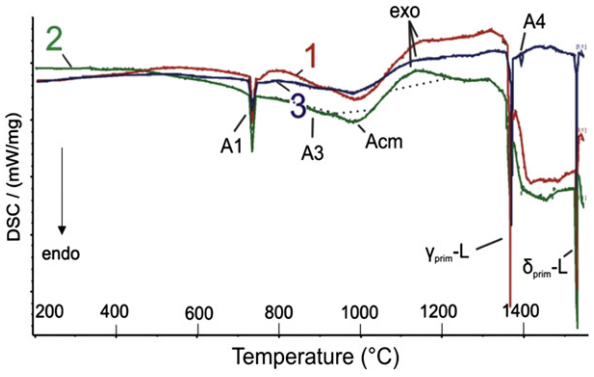

Fig. 11 – DSC heating curves for samples 1 (core), 2 (cutting edge) and 3 (back).

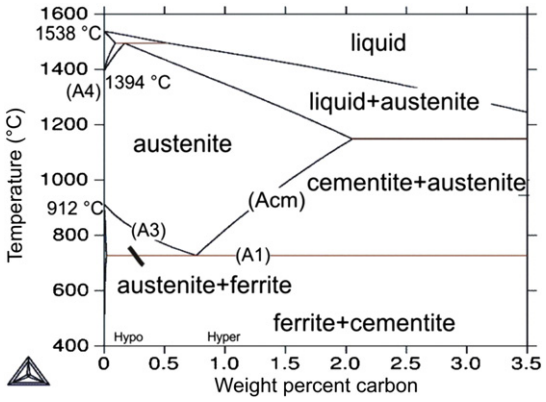

Fig. 12 – Calculated metastable Fe–Fe_3C phase diagram.

Combination of Eqs. (2) – (3) and the mass balance (4) results in following reaction:

$$FeO(s) + CO(g) = Fe(s) + CO_2(g)$$

And the relation for the p_{CO2}/p_{CO} ratio:

$$(a_{Fe}P_{CO2})/(a_{FeO}P_{CO}) = \exp\left(-\left(\left(G^0_{Fe} + G^0_{CO2}\right) - \left(G^0_{FeO} + G^0_{CO}\right)\right)/RT\right) \quad (5)$$

The chemical composition of the potential inclusions is also related to the temperature and partial pressure of the gases present (5).

Nevertheless, all inclusions are heterogeneous and no strict correlation exists between their chemical compositions. The inclusions were probably formed not only from slag but, also from refractory material rich in SiO_2, Al_2O_3, MgO and CaO (Table 3).

Studies on pure iron or Fe–C alloys using thermal analysis may be found in ref. [26–28]. The data were further compared with the metastable Fe–Fe_3C phase diagram, calculated using the ThermoCalc software (TCFE7 thermodynamic database). Additionally, calculated enthalpies (also using ThermoCalc) were used for modelling the combined DSC response from ambient temperature to 1550 °C, Fig. 12.

The calculated DSC heating curve, Fig. 13, for two different compositions (ferritic and carbon-rich regions) displays a complexity relatively similar to that of the experimentally obtained DSC curves. Calculation of the DSC curves was done using the Boettinger and Kattner model [29].

Due to the higher carbon content at the surface layer of the blade, the highest microhardness values of 199–377 HV were measured in this zone (Fig. 5a–c: marks: B, C, D, E). These values correspond to a mainly pearlitic microstructure. The microhardness values decreased in the core to 151–171 HV (Fig. 5a–c: marks: A, F). The microstructure in the core of the blade consisted mainly of ferrite. These results are similar to those found elsewhere [30,31].

The analyses suggest that the weapon was made by an experienced smith. The smith was able to produce a useable blade with a soft, tough core and a harder carburised edge. A similar method of manufacture can be observed in many of the analysed cutting weapons from the Middle Ages and the early Modern Period, including expensive double-edges swords used by the elite troops and aristocracy. The investigated Messer was clearly a plain, inexpensive weapon, but its performance would not have been inferior to most swords used by professional soldiers and men-at-arms. It is worth noting that an almost identical Messer from the Czech Republic displays a very similar microstructure and microhardness values [22,31–33].

Table 4 – Averaged microhardness measurements.

Specimen	Mark	Vickers (HV) Min	Max	Average	Standard Deviation
1	A	180	217	200	11.9
	B	227	248	239	7.0
2	C	321	343	336	7.54
	D	363	377	371	4.3
3	E	199	234	219	12.3
	F	151	171	161	6.6

5. Conclusions

The metallurgical characterization of a medieval Messer sword was performed. Though the investigations were limited

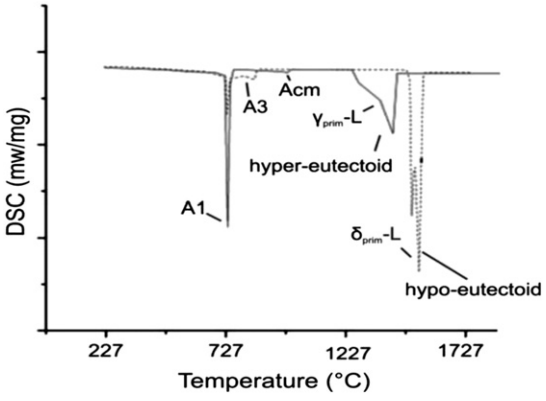

Fig. 13 – Example of a modelled DSC heating curve as the combination of a hypo and hyper eutectoid composition.

to six very small samples taken from three characteristic locations (cutting edge, core and the back) of the blade, the following conclusions can be drawn:

- The sword was manufactured from a single wrought iron billet without intermediate folding or twisting during hammering. After hammering it was carburised and slowly air-cooled to achieve the required mechanical properties. The carbon content and hardness decrease from the surface to the core of the blade. The microstructure in the outer layer is mostly pearlite and in the core mostly ferrite.
- The non-metallic inclusions were derived mostly from slag and some as hammer scale. It is assumed that the slag was probably formed by the so called direct ('bloomery') method which uses iron oxide-enriched slag. The inclusions are of two shapes: some are lump-shaped, but for the most part they are elongated and arranged in strings in a direction perpendicular to the hammering direction.
- The Vickers microhardness results correspond to the observed microstructures.
- A good correlation was found between the recorded and modelled DSC heating curves where, similarly to the observed microstructures, the presence of different microstructural zones was confirmed. The endothermic peaks recorded were typical of zones relatively low in carbon and those enriched in carbon.
- Though the Messer is considered an inexpensive weapon of the masses it was not necessarily an inferior product. The investigated sword has satisfactory mechanical properties entirely comparable to edged weapons used by professional soldiers and even the noble classes. It was evidently well designed and made by a highly skilled craftsman.

Acknowledgment

The authors would like to thank Dr. Peter Kump from Jožef Stefan Institut, Ljubljana, for his help and skill in implementing the EDXRF examinations presented in this study.

REFERENCES

[1] Demmin A. Die Kriegswaffen in ihren geschichtlichen Entwickelungen. Gera: Fr. Eugen Köhler; 1891.
[2] Wagner E, Drobná Z, Tracht Durdík J. Wehr und Waffen des späten Mittelalters. Praha: Artia; 1960 1350–450.
[3] Seitz H. Ein waffenhistorisches Handbuch. Blankwaffen I. Braunschweig: Klinkhardt & Biermann; 1965.
[4] Nickel H. Ullstein Waffenbuch. Eine kulturhistorische Waffenkunde mit Markenverzeichnis. Frankfurt, Berlin, Wien: Ullstein; 1974.
[5] Thomas B, Gamber O. Katalog der Leibrüstkammer I. Wien: Kunsthistorisches Museum; 1976.
[6] Talhoffer H, Rector M. Medieval combat. A fifteenth-century illustrated manual of swordfighting and close-quarter combat. London: Greenhill Books; 2000.
[7] Zabinski G, Walczak B. Codex Wallerstein: a medieval fighting book from the fifteenth century on the longsword, falchion, dagger, and wrestling. Boulder: Paladin Press; 2002.
[8] Müller H, Dürer A. Waffen und Rüstungen. Berlin: Von Zabern; 2002.
[9] Žákovský P. Tesáky ze sbírek Státního hradu Zvíkova. Castellologica Bohem 2008;11:461–72.
[10] Turk P, et al, editor. The Ljubljanica: a river and its past. Ljubljana: Narodni muzej Slovenije; 2009.
[11] Guštin M, editor. Srednjeveško Celje. Ljubljana: Filozofska fakulteta, Oddelek za arheologijo; 2001.
[12] Renoux G, Dabosi F, Lavaud P. Contribution a l'histoire des techniques et de l'armament: essais de restitution du forgeage de pointes de fleche a partir de barres de fer d'epoque antique. Gladius 2009;29:39–70.
[13] Williams A. A metallurgical study of some Viking swords. Gladius 2009;29:121–84.
[14] Eichert S, Mehofer M, Baier R. Archäologische und archäometallurgische Untersuchungen an einer karolingerzeitlichen Flügellanzenspitze aus dem Längsee in Kärnten/Österreich. Archäol Korrespondenzblatt 2011;41:139–54.
[15] Espen Van PJM, Janssens KHA. In: Grieken Van RE, Markowicz AA, editors. Handbook of X-ray spectroscopy: methods and techniques. New York: Marcel Dekker; 1993.
[16] Nečemer M, Kump P, Vogel-Mikuš K. Use of X-ray fluorescence-based analytical techniques in phytoremediation. In: Golubov I, editor. Handbook of phytoremediation, (Environmental science, engineering and technology). New York: Nova Science Publishers; 2011. p. 331–58.
[17] Klančnik G, Medved J, Mrvar P. Differential thermal analysis (DTA) and differential scanning calorimetry (DSC) as a method of material investigation. RMZ-MG, 57; 2010 127–42.
[18] Cvikel D, Ashkenazi D, Stern A, Kahanov Y. Characterization of a 12-pdr wrought-iron cannonball from the Akko 1 shipwreck. Mater Charact 2013;83:198–211.
[19] Aronson A, Ashkenazi D, Barkai O, Kahanov Y. Archeometallurgical investigation of the iron anchor from the Tantura F shipwreck. Mater Charact 2013;78:108–20.
[20] Nečemer M, Lazar T, Kump P, Žužek B. Study of the provenance and technology of Asian Kris Daggers by application of X-ray analytical techniques and hardness testing. Acta Chim Slov 2013;60(2):351–7.
[21] Valério P, Silva RJC, Araújo MF, Soares AMM, Barros L. A multianalytical approach to study the Phoenician bronze technology in the Iberian Peninsula–a view from Quinta do Almaraz. Mater Charact 2012;67:74–82.
[22] Hošek J. Metalografie ve službách archeologie. Praha: Archeologický ústav AV ČR; 2003.
[23] Vella D, Degringy C, Grech M, Williams A. Metallurgy of armour exhibited at the Palace Armoury Valletta, Malta. Proc. of Metal 2004. National Museum of Australia Canberra ACT, October 4-8; 2004.
[24] Blakelock E, Torres MM, Veldhuijzen HA, Young T. Slag inclusions in iron objects and the quest for provenance: an experiment and a case study. J Archaeol Sci 2009;36:1745–57.
[25] Mapelli C, Nicodemi W, Riva RF. Microstructural investigation on a medieval sword produced in 12th century A.D. ISIJ Int 2007;47:1050–7.
[26] Krielaart GP, Brakman CM, Van der Zwaag S. Analysis of phase transformation in Fe-C alloys using differential scanning calorimetry. J Mater Sci 1996;31:1501–8.
[27] Liu YC, Sommer F, Mittemeijer EJ. The austenite-ferrite transformation of ultralow-carbon Fe-C alloys; transition from diffusion-to interface- controlled growth. Acta Mater 2006;54:3383–93.
[28] Li CM, Sommer F, Mittemeijer EJ. Characteristics of $\gamma \rightarrow \alpha$ transformation in Fe-Mn alloys. Mater Sci Eng A 2002;325A:307–19.

[29] Boettinger WJ, Kattner UR. On DTA curves for the melting and freezing of alloys. Metall Mater Trans A 2002;33A:1779–94.
[30] Totten GE. Steel heat treatment2nd ed.; 2007 [Portland, Oregon, USA].
[31] Willams A. A metallurgical study of some Viking swords. Gladius 2009;29:121–84.
[32] Williams A. Methods of manufacture of swords in medieval Europe: illustrated by the metallography of some examples. Gladius 1977;13:75–101.
[33] Edge D, Williams A. Some early medieval swords in the Wallace Collection and elsewhere. Gladius 2003;26:191–210.